Society For Biomaterials

Raman spectroscopic study of remelting and annealing-induced effects on microstructure and compressive deformation behavior of highly crosslinked UHMWPE for total hip arthroplasty

Yasuhito Takahashi,[1,2] Nobuhiko Sugano,[3] Leonardo Puppulin,[1] Wenliang Zhu,[3] Giuseppe Pezzotti[1,4]

[1]Ceramic Physics Laboratory, Kyoto Institute of Technology, Sakyo-ku, Matsugasaki, Kyoto 606–8585, Japan
[2]Department of Orthopaedic Surgery, Tokyo Medical University, 6-7-1 Nishishinjuku, Shinjuku-ku, Tokyo 160-0023, Japan
[3]Department of Orthopaedic Medical Engineering, Osaka University Graduate School of Medicine, 2-2 Yamadaoka, Suita, Osaka 565–0871, Japan
[4]The Center for Advanced Medical Engineering and Informatics, Osaka University, 2–2 Yamadaoka, Suita, Osaka 565–0871, Japan

Received 26 July 2013; revised 24 December 2013; accepted 19 March 2014
Published online 3 April 2014 in Wiley Online Library (wileyonlinelibrary.com). DOI: 10.1002/jbm.b.33164

Abstract: Three-dimensional crystallographic morphologies were studied by means of confocal/polarized Raman spectroscopy as developed upon manufacturing in three different types of first and second generation highly crosslinked UHMWPE (HXLPE) acetabular liners. The impact of such microstructural characteristics on the deformation behavior of the liners was also evaluated and discussed from the viewpoint of molecular chain mobility. All the investigated liners showed similar microstructural transitions within the first 35 μm below their surfaces in terms of crystallinity, molecular orientation, and crystalline anisotropy. Interestingly, different postirradiation heat treatments (remelting or annealing in single step or in sequential steps) led to clear differences in the subsurface microstructure among the three liners. Remelted liner possessed both lower bulk crystallinity and degree of molecular orientation as compared to the annealed liners. Sequentially, irradiated/annealed liner showed the highest degree of crystallinity and orientation among the studied liners. The peculiar microstructure of this latter liner exhibited the highest restoring (shape-recovery) force against the applied uniaxial strain. Accordingly, the present study suggests that the sequential irradiation and annealing offers an efficient way to obtain microstructure quite suitable for attaining high creep resistance. However, all the investigated liners exhibited the significantly low values of surface anisotropy, which could be equally efficient in minimizing strain-softening-assisted wear phenomena. © 2014 Wiley Periodicals, Inc. J Biomed Mater Res Part B: Appl Biomater, 102B: 1762–1770, 2014.

Key Words: polyethylene (UHMWPE), hip prosthesis, crystallinity, morphology, strain

How to cite this article: Takahashi Y, Sugano N, Puppulin L, Zhu W, Pezzotti G. 2014. Raman spectroscopic study of remelting and annealing-induced effects on microstructure and compressive deformation behavior of highly crosslinked UHMWPE for total hip arthroplasty. J Biomed Mater Res Part B 2014:102B:1762–1770.

INTRODUCTION

There has been great interest by the orthopedic community in the development of improved processing methods of highly crosslinked UHMWPE (HXLPE) for hip joint application.[1–8] In particular, the effects of radiation crosslinking have been extensively studied as a means to improve the wear resistance.[6–11] The network structures achieved by crosslinking can resist detachment of polyethylene molecules from the liner surface induced by the chain scission during wear. Irradiation doses in the range of 50–100 kGy are widely accepted for HXLPE acetabular liner.[6–8] Such dose can be also regarded as an upper limit since fatigue crack-propagation resistance, ultimate tensile strength, and elongation at break might eventually decrease.[8,12–14] This negative effect is due, on the microscopic scale, to a loss of chain mobility (i.e., residually strained chains, under microstructural constraints, rather break than deform), which in turn reflects, on the macroscopic scale, in a diminished material ductility.[8,12–14]

In addition to the radiation crosslinking, a postirradiation heat treatment has been commonly conducted since the late 1990s, which enables to minimize the presence of residual free radicals leading to oxidative degradation. It should be noted that a postirradiation remelting [a thermal treatment involving heating up to above the melting temperature (>135°C)] can the most effectively eliminate all the free radicals, but it might also irreversibly change the polyethylene microstructure. On the other hand, a postirradiation annealing below the melting temperature preserves the microstructure, but unavoidably allows for an uncertain amount of residual free radicals to remain trapped in the

Correspondence to: G. Pezzotti (e-mail: pezzotti@kit.ac.jp)

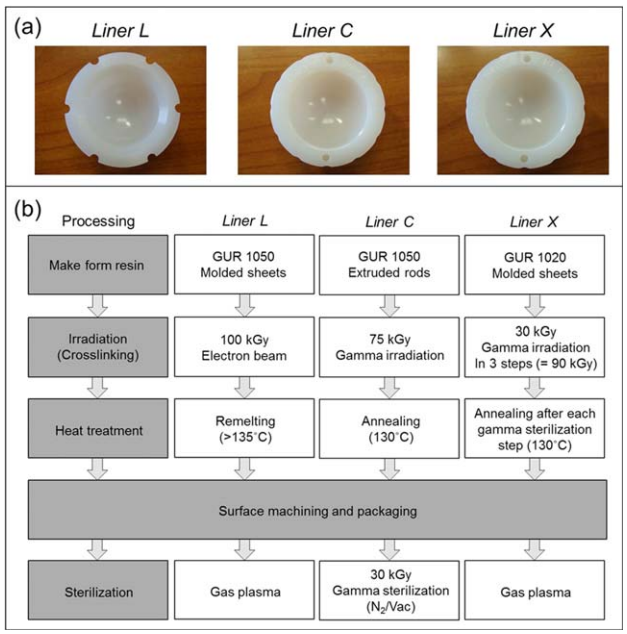

FIGURE 1. Comparison of photographs (a) and processing steps (b) of highly crosslinked UHMWPE acetabular liners investigated in this study. [Color figure can be viewed in the online issue, which is available at wileyonlinelibrary.com.]

final product, thus increasing the risk of *in vivo* oxidation. We have briefly summarized above the main concepts underlying the present understanding of HXLPE acetabular liners (i.e., especially the yet existing dualism annealing vs. remelting), but very few evidences have yet been quantitatively shown to clarify the actual polyethylene microstructures at the molecular scale in biomedical implants. Therefore, the optimum microstructure for HXLPE joint prostheses has not yet been individuated and the choices of different thermal treatments are still argument of controversies among implant makers. In the above context, the purpose of this study is twofold:

i. To investigate the three-dimensional crystalline morphology, the degree of molecular alignment, and compressive deformation behavior of HXLPE acetabular liners manufactured either by remelting or by annealing processes.
ii. To discuss the distinctive microstructural patterns produced through different manufacturing choices and their possible implications to the *in vivo* performance of the liners.

MATERIAL AND METHODS

Investigated HXLPE acetabular liners

This study examines the three types of HXLPE acetabular liners that were prepared according to different manufacturing procedures [Figure 1(a)]. Of the three investigated liners, one was remelted after electron beam radiation (henceforth referred to as *Liner L*), while the remaining two (*Liners C* and *X*) were both annealed after gamma-ray irradiation, according to a single step or to a sequential number of steps. A schematic description of the processing procedures for the preparation of each investigated liner is given in Figure 1(b).

Liner L was Longevity^{TM}, produced by Zimmer (Warsaw, IN), which belongs to the first-generation of HXLPE liner. This liner has been clinically introduced since 1999. GUR 1050 (5.5–6 million g/mol) compression molded sheets was radiation-crosslinked by electron beam with a total dose of 100 kGy and then remelted (>135°C) to quench residual free radicals.

Liner C was Crossfire^{TM}, produced by Stryker Orthopedics. (Mahwah, NJ), which also belongs to first-generation of HXLPE liner. This liner has been clinically introduced in 1998. The manufacturing procedure of *Liner C* also starts from GUR 1050 extruded rod. The rod was gamma-irradiated with a nominal dose of 75 kGy and subsequently annealed at 130°C. After being machined into the shape of acetabular liner and then barrier packaged, *Liner C* was exposed again to gamma irradiation for sterilization purposes, with the nominal dose of 30 kGy in nitrogen atmosphere.

Liner X was X3^{TM}, produced by Stryker Orthopedics, and belongs to a second-generation of HXLPE liner. This liner has been clinically introduced since 2005. GUR 1020 (3.5 million g/mol) compression molded sheets were radiation-crosslinked by the nominal dose of 30 kGy and then annealed at 130°C. The same procedure is sequentially repeated three times (i.e., the cumulative radiation dose being 90 kGy) with the expectation that, for the same cumulative radiation dose, a more pronounced crosslinking formation could take place with a free radical concentration conspicuously lower than a standard (single) irradiation/annealing procedure.

Confocal/polarized Raman spectroscopy to analyze molecular structures

All the spectroscopic assessments in this study were made by means of a Raman microprobe spectrometer (T-64000, Horiba/ Jobin-Yvon, Kyoto, Japan) in back-scattering geometry. The excitation source was a 488.0 nm Ar-ion laser (Stabilite 2017-Spectra Physics, Mountain View, CA) yielding a power of ~35 mW on the HXLPE liner surfaces. Deconvolution of all the recorded Raman spectra into sub-bands was achieved according to automatic fitting algorithms contained in commercially available computational software (Labspec 3, Horiba/Jobin-Yvon, Kyoto, Japan). Mixed Gaussian/ Lorentzian curves were used throughout the spectral fitting computations.

The confocal configuration of the probe adopted throughout the present experiment corresponded to a ×100 objective; numerical aperture (N.A.), focal length, and pinhole diameter were fixed as 0.7, 6.0 mm, and 100 μm, respectively. Individual spectra were typically collected in 10 s in both polarized and nonpolarized measurements. The recorded spectra were averaged over three successive measurements. A spectral resolution of 0.40 cm^{-1} was achieved by means of an 1800 l/mm grating. Spectral mapping was nondestructively performed in order to characterize crystallinity from the surface down to 100 μm inside of the liners. A spectral map (50 × 50 μm^2 in dimension) was collected at each depth, z_{lab}, with an in-plane sampling of 2.5 μm steps (for a total of 1323 spectra per each map). The average value of the map was assumed to be the crystallinity value at each selected depth. During the polarized

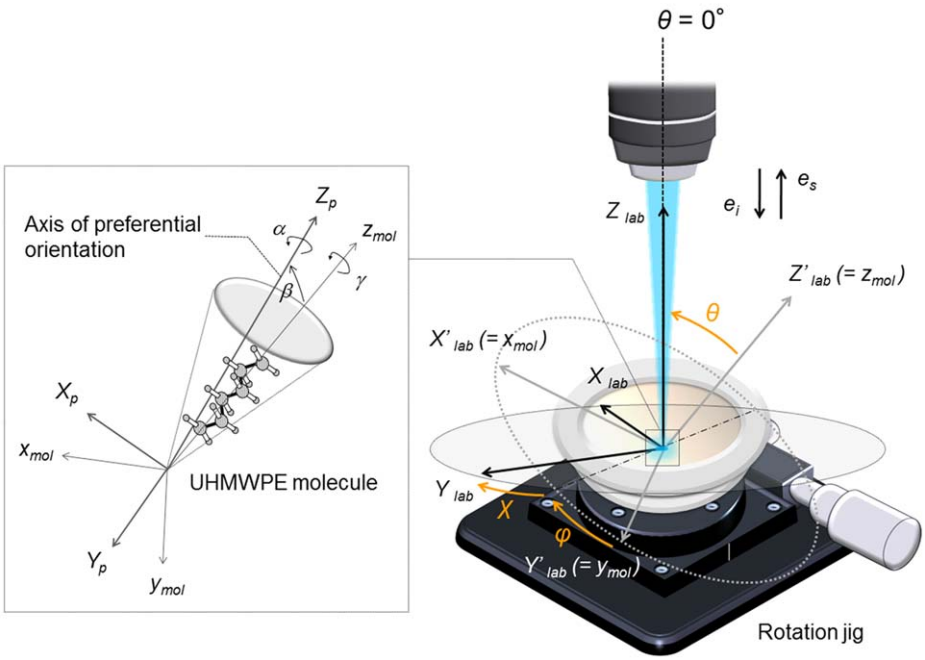

FIGURE 2. Schematic of our choice of Cartesian reference systems and of the Euler angles governing their rotations in space, as explained in the section of THEORY AND CALCULATIONS. [Color figure can be viewed in the online issue, which is available at wileyonlinelibrary.com.]

measurements conducted for the assessment of molecular orientation, a parallel polarization filter and a half-wave plate were placed between liners and detector, which were set to pass the scattered Raman radiation horizontally to a CCD camera. A schematic of the spectroscopic measurement protocol is given in Figure 2. The liners were placed on a rotation jig and polarized Raman spectra were collected at 19 different azimuthal angles within the interval $0 \leq \chi \leq 180^{\circ}$, with sequential in-plane rotational steps of 10°. The focal plane was eventually shifted toward the material inside in order to nondestructively screen the subsurface regions of the liners. Mathematical data treatment, according to the theory described in specific publications,[15–17] was performed with the aid of commercially available software (Mathematica 7; Wolfram Research, IL). In the conventions adopted for this study, θ_p represents the out-of plane tilt angle with respect to the local direction parallel to the surface plane of the polyethylene bearing. The details of the theoretical backbone of this article are briefly summarized in the section of THEORY AND CALCULATIONS.

Characterization of residual deformation properties and chain mobility

In the present study, we compare the time-dependent deformation of *Liner L*, *C*, and *X* as obtained by uniaxial relaxation tests followed by strain recovery, which takes place in a non-negligible amount. The amount of strain recovery is an important parameter in the deformation of HXLPE liners, because it has a direct impact on the amount of residual plastic deformation stored during service and it is a direct measure of the molecular chain mobility available in the engineered HXLPE microstructure. In these tests, a residual plastic deformation was induced in samples purposely prepared by cutting the acetabular liners as received from the maker into rectangular prisms $4 \times 4 \times 8$ mm^3 in dimension. The samples were obtained from the bottom area of the liner. Furthermore, particular care was taken in order to smooth down only the four corners of the slightly concave surface of the sample. This latter procedure enabled us to flatten the originally concave surface to match the compressive surface of the jig while preserving the original microstructure of acetabular component at the central area of the sample, thus reproducing as closely as possible the conditions encountered during *in vivo* loading. One-dimensional relaxation tests were performed using the uniaxial compressive jig. The residual strain in each as-received material was assumed as $\varepsilon = 0$ and an increasing compressive load was applied stepwise. At each step the material was subjected to a sudden compressive strain of a predetermined magnitude, which was kept constant for at least 24 h in order to allow the full development of internal deformation allowed by the microstructure. The load was then released and the sample allowed recovering of its inelastic strain for at least 24 h, a time interval sufficient to obtain a nearly full recovery, especially at low and moderate levels of deformation, as in the case of the present investigation.[18,19] At each step, the engineering strain was measured along the sample long axis by means of a micrometer caliper both before and after recovery, henceforth referred to as ε_i and ε_f, respectively.

THEORY AND CALCULATIONS

For the assessment of crystallinity (α_c) of HXLPE liner, we used the intensity of vibrational bands located at 1296, 1310, and 1418 cm^{-1}, as obtained from unpolarized Raman spectra.

A broad band at 1310 cm^{-1}, which is assigned to the amorphous phase of the polymer, results from C—C twisting vibrational mode. On the other hand, the bands at 1296 and 1418 cm^{-1}, which arise from the crystalline phase, possesses CH_2 twisting and bending modes, respectively. Computation of α_c was made according to the following equation[20,21]:

$$\alpha_c = \frac{I_{1418}}{0.46(I_{1296}+I_{1310})} \tag{1}$$

where I is the integrated intensity of the Raman band whose wave number is identified by the subscript.

For the assessments of preferential molecular orientation (θ_p) and its orientational order ($<P_2(\cos\beta)>$), we analyzed the polarized spectroscopic behavior of the Raman band located at 1130 cm^{-1}, which is related to the C—C stretching vibration ($A_g + B_{1g}$ mode). For individual polyethylene molecule, the parallel polarization intensity ($I^{||}_{exp}$) on crystallographic orientation (i.e., the *c*-axis orientation of the orthorhombic structure) was expressed in terms of Euler angles (θ, φ, χ) and Raman tensor parameters ($a = 0.260$, $b = 0.202$, $c = -0.898$, and $d = -0.664$) as[15–17]:

$$I^{||}_{A_g+B_{1g}} = \Lambda\left\{\begin{array}{c}\nu[c\sin^2\theta\sin^2\chi + a(\sin\varphi\cos\chi+\cos\theta\cos\varphi\sin\chi)^2 + b(\cos\varphi\cos\chi-\cos\theta\sin\varphi\sin\chi)^2]^2 \\ +(1-\nu)[-2d(\sin\varphi\cos\chi+\cos\theta\cos\varphi\sin\chi)(\cos\varphi\cos\chi-\cos\theta\sin\varphi\sin\chi)]^2\end{array}\right\}+\Gamma \tag{2}$$

In Eq. (2), Λ and Γ represent numerical constants that only depend on the instrumental configuration and on the spectral band employed; $\nu$is a fitting parameter that takes into account the contribution of A_g mode to the observed Raman band. On the other hand, the statistical molecular distribution around preferential orientation axis can be described by means of orientation distribution function (ODF, $f(\beta)$). Taking into sum of the scattering intensity from all the individual molecules exist within the volume of laser probe, the overall polarized Raman intensity ($I^{||}_{exp}$) for HXLPE products is provided as[15–17]:

$$I^{||}_{exp} = \frac{\int_{\gamma=0}^{\gamma=2\pi}\int_{\alpha=0}^{\alpha=2\pi}\int_{\beta=0}^{\beta=2\pi} I^{||}_{A_g+B_{1g}}(\theta,\varphi,\chi)f(\beta)\sin\beta d\beta d\alpha d\gamma}{\int_{\gamma=0}^{\gamma=2\pi}\int_{\alpha=0}^{\alpha=2\pi}\int_{\beta=0}^{\beta=2\pi} f(\beta)\sin\beta d\beta d\alpha d\gamma} \tag{3}$$

where θ and χ, were expressed as functions of a new set of Euler angles (θ_p, φ_p, χ_p) locating the (average) preferential axis of the polymeric chains, according to the following equations (derived by means of simple Euler angle rotational transformations in space[15–17]):

$$\theta = \arccos[\cos\beta\cos\theta_p - \cos(\alpha+\varphi_p)\sin\beta\sin\theta_p] \tag{4}$$

$$\begin{aligned}\chi = \arcsin\{&[\cos\alpha\cos\chi_p\sin\beta\sin\varphi_p + \sin\chi_p \\ &(\cos\beta\sin\theta_p - \cos\theta_p\sin\alpha\sin\beta\sin\varphi_p) \\ &+\cos\varphi_p\sin\beta(\cos\chi_p\sin\alpha - \cos\alpha\cos\theta_p\sin\chi_p)]/ \\ &\sqrt{1-[\cos\beta\cos\theta_p - \cos(\alpha+\varphi_p)\sin\beta\sin\theta_p]^2}\}\end{aligned} \tag{5}$$

where the independent set of Euler angles (α, β, γ) describes the rotations in space of the Cartesian frame integer to the molecular orientation axes, ($x_{mol}y_{mol}z_{mol}$), within the polarized Raman probe, with respect to the axes of preferential orientation of the molecular structure, (x_p, y_p, z_p) (cf. Figure 2). The orientation distribution function, $f(\beta)$, was then set as[22–24]:

$$f(\beta) = A\exp\{-[\lambda_2 P_2(\cos\beta)+\lambda_4 P_4(\cos\beta)]\} \tag{6}$$

where A is a constant and the parameters λ_2 and λ_4 are referred to as Lagrange multipliers.[23,24] Note that in the computational procedure, we considered the Euler angle, φ, as a constant equal to φ_p, namely, we neglected any torsional rotation of the molecular chains around their *c*-axis of the crystalline cell. In addition, we assumed the existence of a uniaxial symmetry with respect to the preferential orientation of the molecular chains, which is only dependent on one polar angle, β (Figure 2) (i.e., angle, α and γ do not enter the expression of molecular distribution).

A mathematical procedure was performed by using Eqs. (2–6) to find the best-fitting curves to a data set of polarized Raman intensity collected at different *in-plane* orientation (χ). After the computational routine, θ_p and $f(\beta)$ can be determined, and the degree of molecular orientation also can be calculated using the following equation.[23,24]

$$\int_{\gamma=0}^{\gamma=2\pi}\int_{\alpha=0}^{\alpha=2\pi}\int_{\beta=0}^{\beta=2\pi} f(\beta)\sin\beta d\beta d\alpha d\gamma = 1 \quad (f(\beta)\geq 0) \tag{7}$$

$$\int_{\gamma=0}^{\gamma=2\pi}\int_{\alpha=0}^{\alpha=2\pi}\int_{\beta=0}^{\beta=2\pi} P_2(\cos\beta)f(\beta)\sin\beta d\beta d\alpha d\gamma = \langle P_2(\cos\beta)\rangle \tag{8}$$

where $<P_2(\cos\beta)>$ represents the degree of molecular orientation called Harmans' orientation parameter. Its value 0 indicates that the molecular orientation is fully random (isotropic), while value 1.0 represents a perfect orientation to the preferential orientation axis, respectively. For the partial molecular orientation, the value should be $0 < (I^{||}_{exp}) < 1.0$. The Hermans' orientation parameter can thus be considered as a quite indicative parameter for quantifying the

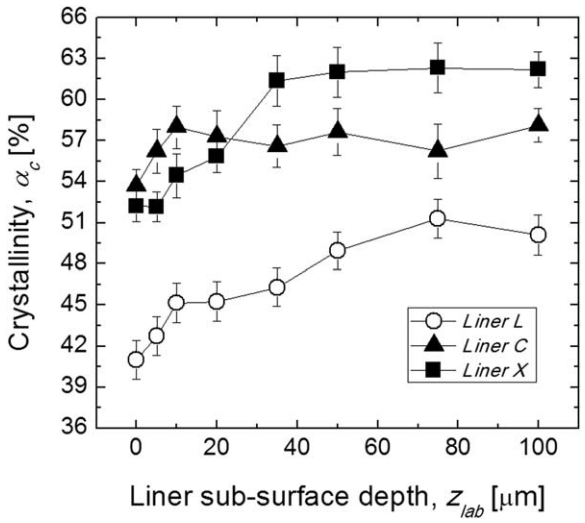

FIGURE 3. Depth profiles of crystallinity (α_c) investigated in the as-received *Liner L*, *C*, and *X*.

degree of molecular alignment in UHMWPE crystalline lamellae.

EXPERIMENTAL RESULTS

Depth profiles of crystallininity

Crystallinity (α_c) was calculated using Eq. (1) as given in the previous section. Figure 3 represent the depth profiles of average α_c as detected in *Liner L*, *C*, and *X*. As seen, the α_c values on the surfaces ($z_{lab} = 0$), which were always lower than those in the subsurface regions, lie between 40 and 54%, being the lowest in *Liner L*. On the other hand, *Liner C* and *X* showed the similar values of surface α_c. In addition, all the liners experienced a nonlinear gradient of α_c along the first 35 μm toward the subsurface, after which the profiles reached a nearly constant value. The lowest α_c value measured in the bulk of remelted *Liner L* was 51.3%, while the bulk α_c value in *Liner X* was the highest (62.3%) among all liners. The α_c of *Liner C* reached nearly constant in its bulk at an intermediate value of about 57.3%.

Stereological arrangement at the molecular scale

Figures 4(a–d) show the angular dependences of normalized Raman intensities as obtained along the subsurface depth of *Liner L*, *C*, and *X*. Pronounced differences among different liners could be noticed in both intensity variation and periodicity (from 180° to 90°) of the angular profiles. Figure 5 shows the depth profiles of the zenithal angle, θ_p, (cf. Figure 2) describing the preferential (average) molecular orientation in the laboratory coordinate system, as calculated from the best fitting of the data set in Figure 4. The salient notions that can be extracted from the plots in Figure 5 can be summarized as follows:

(i) In all types of liners, the molecular chains at the surface are mainly aligned along a direction parallel to the liner surface ($\theta_p = 90°$), but these tend to reach the direction perpendicular to the surface ($\theta_p = 0°$) with proceeding along the subsurface. The common trend of orientation parallel to the surface is interpreted as being a direct consequence of the machining process.

(ii) In the annealed *Liner C* and *X*, quite similar trend of preferential molecular orientation angles was observed along the subsurface, and these depth variations from parallel to perpendicular to the liner surface more quickly occur within the first 20 μm along the subsurface, as compared to *Liner L*.

Orientation distribution functions (ODF) and degree of molecular orientation

The ODFs, $f(\beta)$, obtained along the depth direction are shown in Figure 6a–c for *Liner L*, *C*, and *X*, respectively. The interpretation of the complex data patterns in Figure 6 can be facilitated by noting that, for the same preferential orientation angle, θ_p, the broader the ODF the less statistically aligned the structure. With this understanding in mind, it immediately appears evident that *Liner X* exhibited significantly sharper $f(\beta)$ as compared to both *Liners L* and *C*, thus experiencing by far the most statistically aligned structure. The results of the calculation based on the formalism described in the above section are given in terms of plots $<P_2 (\cos \beta)>$ vs. z_{lab} in Figure 7. The salient notions obtained from the plots in Figures 6 and 7 can be summarized as follows:

(i) Surface degree of molecular orientation observed in *Liner L*, *C*, and *X* showed an in-plane trend that is quite close to randomness ($0.13 << P_2 (\cos \beta) >< 0.20$).

(ii) Upon proceeding toward the liner depth, we recorded a relatively steep (i.e., within an interval $\Delta z_{lab} \approx 20$ μm) increase in the statistical degree of alignment of *Liner X* (up to $<P_2 (\cos \beta)> = 0.51$), while only a slight increase in degree of alignment with increasing z_{lab} was found in *Liner L* (up to $<P_2 (\cos \beta)> = 0.38$). The trend recorded in *Liner C* was somewhat intermediate between the two above types of liner (up to $<P_2 (\cos \beta)> = 0.43$).

Compressive deformation and strain recovery behavior

Mechanical properties are expected to vary depending on microstructure and anisotropy of UHMWPE. Figure 8 shows plots of true strain after recovery, ε_f, as a function of externally applied strain, ε_i, for *Liner L*, *C*, and *X*. For all the investigated liners, the results revealed a linear dependence between ε_f and ε_i, but also a clear difference in the slopes of the three fitting lines. In fact, *Liner L* showed the highest slope ($\varepsilon_f/\varepsilon_i = 0.52$), *Liner C* an intermediate value ($\varepsilon_f/\varepsilon_i = 0.46$), while *Liner X* possessed the lowest slope ($\varepsilon_f/\varepsilon_i = 0.42$).

DISCUSSION

Confocal/polarized Raman spectroscopy clearly confirmed that all the obtained microstructural parameters (α_c, θ_p, $<P_2 (\cos \beta)>$) showed gradual transitions from surface down to subsurface regions (cf. Figures 3, 5, and 7) within the first 35 μm below their surfaces. A lower crystallinity and

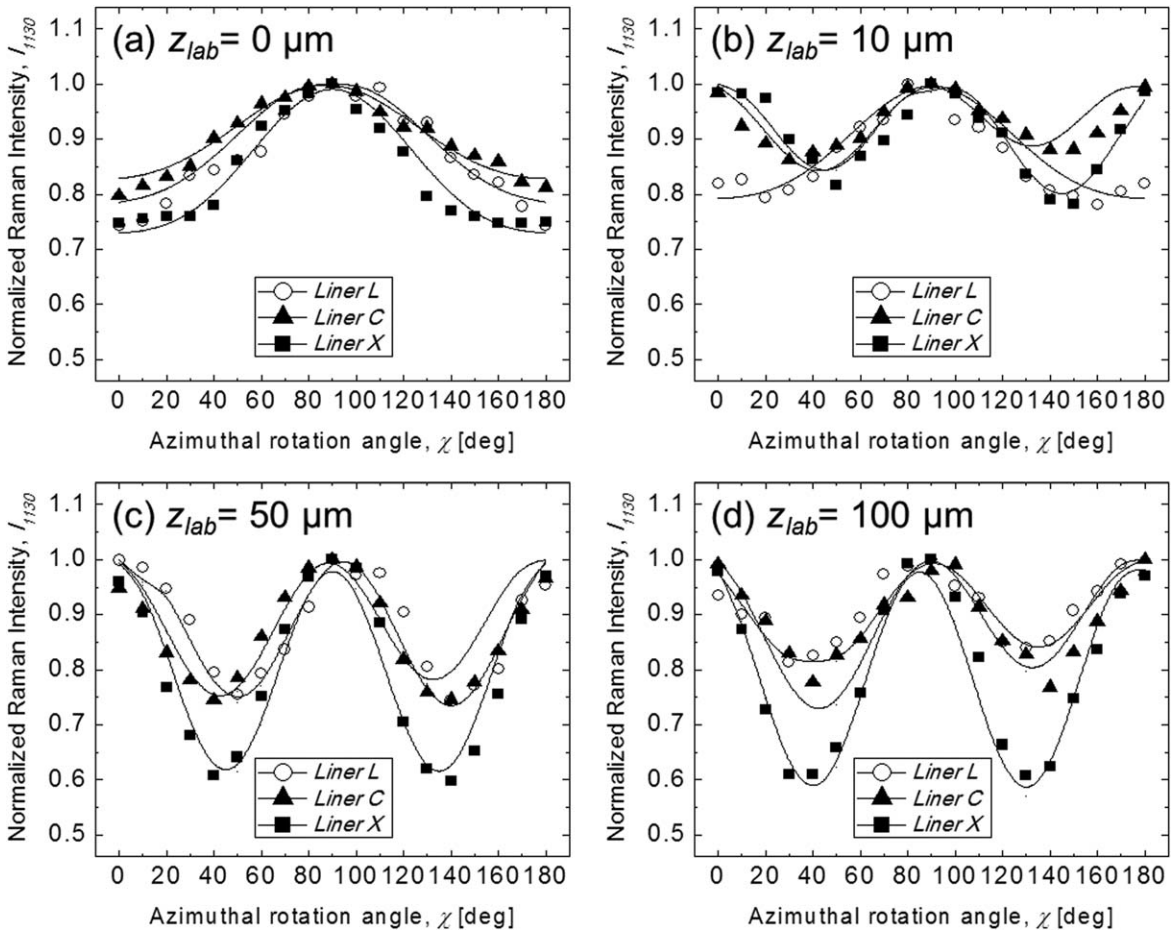

FIGURE 4. Experimental plots of the angular dependence of polarized Raman scattering intensities recorded upon in-plane rotation, χ, at different depth of the as-received *Liner L*, *C*, and *X*. Full lines represent the results of best fitting to the experimental data according to Eq. (3).

anisotropy were found in the same regions as compared to their bulks, indicating an effect of decrystallization induced by surface finishing (i.e., lathe machining and polishing). Moreover, the near-surface molecular orientation parallel to the articulating surface also can be the structural evidence for initial existence of plasticity layer formed in the manufacturing stages. The differences of the maximum α_c values can be interpreted mainly as a consequence of the post-irradiation heat treatments [i.e., a reduced crystallinity by remelting (in *Liner L*) vs. substantial preservation of the as-irradiated structure upon annealing (in *Liner C* and *X*)]. In fact, the annealed *Liner C* and *X* differ by about 5% in their bulks despite annealing combined with a comparable dose of gamma-irradiation, which can be mainly related to the difference of the selected types of starting resin (i.e., GUR 1050 vs. GUR 1020). In the unirradiated and unheated states, the average α_c values of compression molded GUR 1050 and GUR 1020 were reported as 45.0 and 51.6%, respectively.[25] The high fraction of crystalline phase in the *Liner X* is expected to lead to an improved strength and deformation resistance.

According to the strain-recovery behavior shown in Figure 8, the microstructure of *Liner X* is more resistant to plastic deformation as compared to *Liner L* and *C*, considering that for the same applied constant strain, ε_i, the three-step annealed material showed a higher capacity of recovery, thus incorporating a lower amount of residual plastic

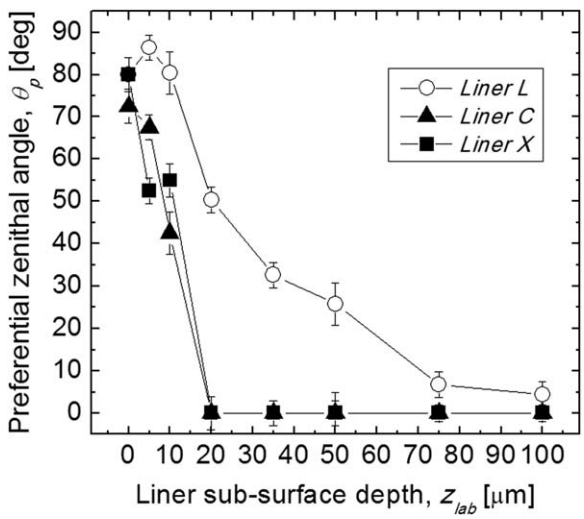

FIGURE 5. Depth profiles of the preferential (average) molecular orientation (θ_p) investigated in the as-received *Liner L*, *C*, and *X*.

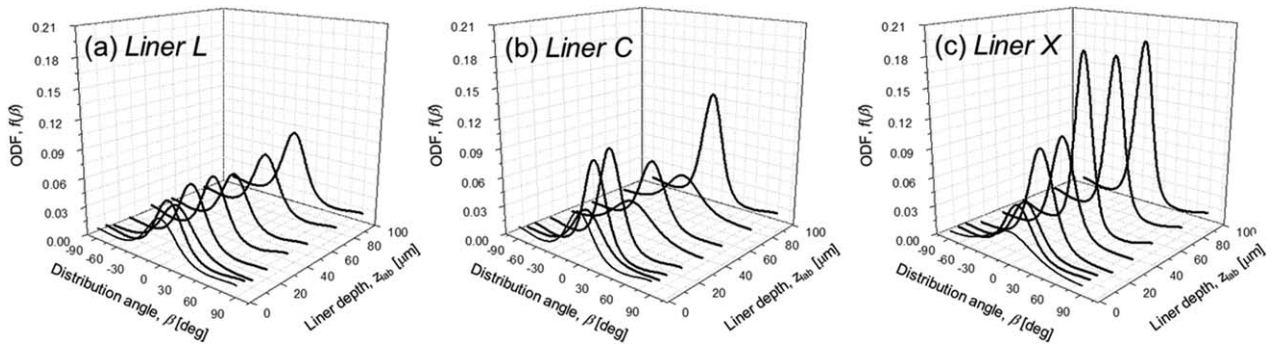

FIGURE 6. Orientation distribution functions (ODFs, $f(\beta)$) calculated at the different depth of the as-received liners [(a–c) for *Liner L*, *C*, and *X*, respectively].

strain, ε_f. The ability to recover is actually enhanced by a higher crystalline phase content. Nevertheless, the improved resistance to compressive strain observed in *Liner X* might be relevant to the difference in not only higher crystallinity, but also a higher degree of molecular orientation (cf. Figures 6 and 7) and crosslink density.[4,26] It is well recognized that an increased degree of crosslinking restricts the mobility of the molecular chain in the amorphous region, thus resisting molecular reorientation during compressive loading (i.e., increased ability to undergo shape recovery after plastic deformation).

Schematic drafts that attempt to summarize the stereological assembly of the molecular structure for *Liner L*, *C*, and, *X* are given in Figure 9. We shall refer to these simplified drafts for the purpose of interpreting the impact of the observed microstructural features on the wear and creep deformation of the studied liners.

As far as the molecular orientation patterns of HXLPE acetabular liner is concerned, early studies by Wang et al.[27,28] already documented in great details the interactions between contact stresses and the molecular structure of worn polyethylene surfaces. A strain softening-assisted adhesive wear model was proposed by which those researchers have successfully clarified how crystalline anisotropy in the UHMWPE structure (i.e., as induced by different modes of sliding) could be responsible for a molecular reorganization process at the wear surface during sliding. This process is driven by plastic strain accumulation at the surface and arises from repeated cyclic asperity contact. Unlike simply linear sliding contacts, in which UHMWPE molecules are stretched along the direction of sliding and undergo significant strain hardening, in multidirectional sliding contact such as that experienced in the natural human joints, molecular orientation actually leads to strain softening and weakening of the liner surface. According to this model, the mechanism of wear debris generation in UHMWPE (in the absence of third-body particles) can be described as the sequential combination of rupture of transversely softened (oriented) molecular chains and shear rupture with formation of fibrillar wear debris. From the microstructural viewpoints, this suggests that a lesser surface orientation (higher degree of orientational randomness) is preferable to alleviate strain-softening-assisted wear in the case of hip joint component. In addition, the adequately high crosslink density in amorphous regions, which can resist crystalline orientation during wear, is necessary to preserve its structure with low anisotropy for a long period

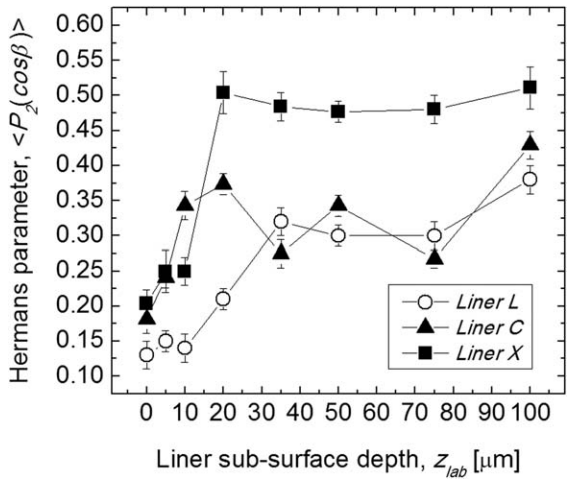

FIGURE 7. Depth profiles of degree of molecular orientation (Hermans parameter, $<P_2(\cos\beta)>$) investigated in the as-received *Liner L*, *C*, and *X*.

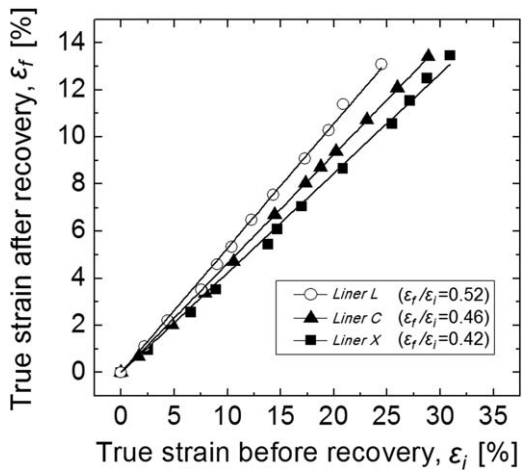

FIGURE 8. Experimental plots of the compressive deformation and shape-recovery behavior of the as-received *Liner L*, *C*, and *X*.

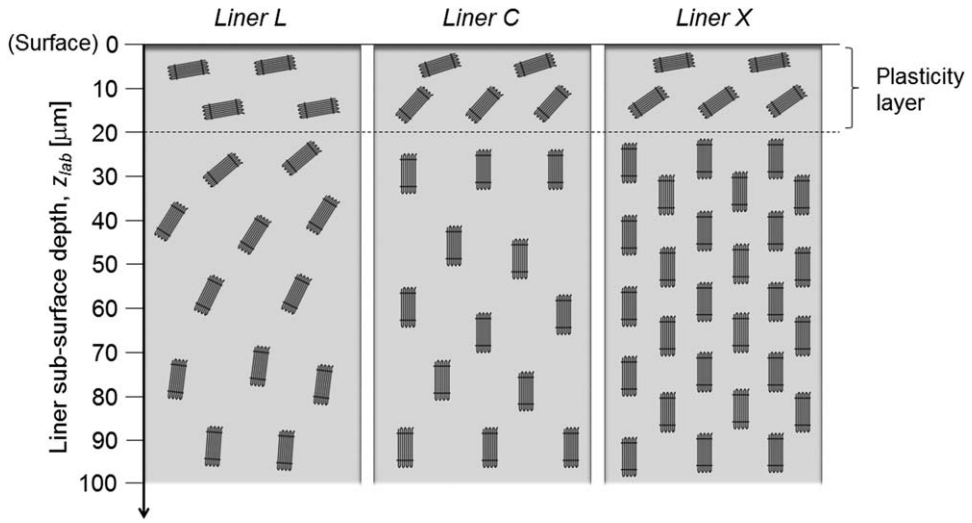

FIGURE 9. Structure models for the as-received *Liner L*, *C*, and *X*, which represent the preferential (average) orientation of UHMWPE molecular chains. Plasticity layers induced by machining were observed in the near-surface regions within $z_{lab} \approx 20$ μm of *Liner L*, *C*, and *X*.

of *in vivo* time. In the current study, all the investigated liners, which are highly crosslinked polyethylene, exhibited a comparably low degree of surface molecular alignment which is likely due to a consequence of surface machining process. Therefore, highly crosslinked *Liners L, C,* and *X* could all be equally efficient in minimizing microscopic wear phenomena as aforementioned.

Recent hip simulator studies with 32 mm Trident acetabular components showed the improved wear performance in *Liner X* in comparison with *Liner C*, and the volumetric wear rates were 3.6 and 1.3 mm^3/million cycles for *Liner C* and *X*, respectively.[3,26] Thus, *Liner X* has ~62% lower rate in *in vitro* wear than *Liner C*. In addition, early clinical studies showed that the *in vivo* wear rates were 0.036[29] and 0.015 mm/year[30] for *Liner C* and *X*, respectively. It indicates that the *in vivo* wear of *Liner X* is about 58% lower than that of *Liner C*. Nevertheless, long-term clinical studies of *Liner X* are still underway, and a concern arises from its less oxidative stability compared to the remelted *Liner L*, due to the existence of residual free radicals (even at the substantially low concentration, $<9.0 \times 10^{14}$ spins/g[5,26]) in its microstructure. As a matter of fact, wear rates of *Liner L* was reported as 0.005 mm/year with 28 mm femoral heads,[31] and 0.007 mm/year with 32 mm Trilogy acetabular components at 8-year follow-up.[32] Direct comparison of wear rates among these three liners is actually beyond the scope of this study, and longer clinical studies are required for an accurate comparison.

Creep resistance of UHMWPE is mainly dependent on its crystallinity, crosslink density, and also bulk anisotropy. Concerning the effect of the degree of crystallinity in polyethylene structures on the macroscopic deformation behavior of the material, high volume fraction of rigid crystalline phase is known to lead to a high resistance against creep deformation. On the other hand, a substantial reduction in the magnitude of creep deformation should be observed in highly oriented UHMWPE microstructures (i.e., rather than in isotropic ones), according to the study by Philip et al.[33] Moreover, they confirmed less creep deformation in a molecular orientation pattern of UHMWPE with the long polymeric chains parallel to the applied stress component, because of an increased stiffness as compared to a perpendicular orientation. In our microstructural models, as shown in Figure 9, *Liner X* possesses the highest perpendicular molecular orientation in its bulk regions below the articular surface, which could be considered as the preferable orientation pattern in order to maximize (compressive) creep resistance. Data in Figures 3–7 clearly demonstrate that *Liner X* possesses a surface microstructure oriented in plane ($\theta_p = 90^\circ$) with a random texture and its bulk regions have a quite high crystalline structure ($(\alpha_c)_{max} = 62.3\%$) perpendicularly oriented with respect to the articular surface ($\theta_p = 0^\circ$) with a high degree of molecular alignment. The positive effects of these microstructural improvements is reflected, in Figure 8, in an improved restoring (i.e., shape-recovery) force against the applied uniaxial strain, which should be considered as the important features in minimizing the risk of femoral head migration *in vivo*.

CONCLUSION

The impact of the selected heat treatments (included either remelting or annealing procedures) after ionizing radiation on the HXLPE microstructure was nondestructively evaluated by confocal/polarized Raman spectroscopy. Our data indicates that remelting procedure decreased both crystallinity and degree of molecular orientation, while annealing procedures preserved (or increased in the case of three-step annealed liner). In addition, these effects provided the difference of shape-recovery force against the applied uniaxial compressive strain. The present study suggests that the sequential irradiation and annealing offers an efficient way to obtain microstructure quite suitable for attaining high creep resistance. However, all the investigated liners

exhibited the significantly low values of surface anisotropy, which could be equally efficient in minimizing strain-softening-assisted wear phenomena.

REFERENCES

1. Kurtz SM, Orhum OK, Evans M, Edidin AA. Advances in the processing, sterilization, and crosslinking of ultra-high molecular weight polyethylene for total joint arthroplasty. Biomaterial 1999; 20:1659–1688.
2. Kurtz SM, Mazzucco D, Rimnac CM, and Schroeder D. Anisotropy and oxidative resistance of highly crosslinked UHMWPE after deformation processing by solid-state ram extrusion. Biomaterial 2006;27:24–34.
3. Dumbleton JH, D'Antonio JA, Manley MT, Capello WN, Wang A. The basis for a second-generation highly crosslinked UHMWPE. Clin Orthop Relat Res 2006;453:265–271.
4. Wang A, Zeng H, Yau SS, Essner A, Manley M Dumbleton J. Wear, oxidation, and mechanical properties of a sequentially irradiated and annealed UHMWPE in total joint replacement. J Phys D Appl Phys 2006;39:3213–3219.
5. Morrison ML, Jani S. Evaluation of sequentially crosslinked ultra-high molecular weight polyethylene. J Biomed Mater Res B Appl Biomater 2009;90:87–100.
6. Oonishi H, Kuno M, Tsuji E, Fujiwara A. The optimum dose of gamma radiation-heavy doses to low wear to low wear polyethylene in total hip prostheses. J Mater Sci: Mater Med 1997;8: 11–18.
7. Muratoglu OK, Bragdon CR, O'Connor DO, Jasty M, Harris WH, Gul R, McGarry F. Unified wear model for highly crosslinked ultra-high molecular weight polyethylenes (UHMWPE). Biomaterial 1999;20:1463–1470.
8. McKellop H, Shen F, Lu B, Campbell P, Salovey R. Development of an extremely wear-resistant ultra high molecular weight polyethylene for total hip replacement. J Orthop Res 1999;17:157–167.
9. Oonishi H, Saito M, Kadoya Y. Wear of high-dose gamma irradiated polyethylene in total joint replacement-Long term radiological evaluation. In Transaction of the 44th Annual Meeting of the Orthopaedic Research Society, New Orleans, LA; 1998. p. 17.
10. Digas G, Karrholm J, Thanner J, Malchau H, Herberts P. The Otto Aufranc Award. Highly cross-linked polyethylene in total hip arthroplasty: randomized evaluation of penetration rate in cemented and uncemented sockets using radiostereometric analysis. Clin Orthop Relat Res 2004;429:6–16.
11. Dorr LD, Wan Z, Shahrdar C, Sirianni L, Boutary M, Yun A. Clinical performance of a Durasul highly corss-linked polyethylene acetabular liner for total hip arthroplasty at five years. J Bone Joint Surg Am 2005;87:1816–1821.
12. Zhao Y, Luo YX, Jiang BZ. Effect of irradiation on crystallinity and mechanical properties of ultrahigh molecular-weight polyethylene. J Appl Polym Sci 1993;50:1797–1801.
13. Lewis G. Properties of crosslinked ultra-high-molecular-weight polyethylene. Biomaterials 2001;22:371–401.
14. Oral E, Malhi AS, Muratoglu OK. Mechanism of decrease in fatigue crack propagation resistance in irradiated and melted UHMWPE. Biomaterials 2006;27:917–925.
15. Takahashi Y, Puppulin L, Zhu W, Pezzotti G. Raman tensor analysis of ultra-high molecular weight polyethylene and its application to study retrieved hip joint components. Acta Biomater 2010;6: 3583–3594.
16. Puppulin L, Takahashi Y, Zhu W, Pezzotti G. Raman polarization analysis of highly crystalline polyethylene fiber. J Raman Spectrosc 2011;42:482–487.
17. Puppulin L, Takahashi Y, Zhu W, Sugano N, Pezzotti G. Polarized Raman analysis of the molecular rearrangement and residual strain on the surface of retrieved polyethylene tibial plates. Acta Biomater 2010;7:1150–1159.
18. Meyer RW, Pruitt LA. The effect of cyclic true strain on the morphology, structure, and relaxation behavior of ultra high molecular weight polyethylene. Polymer 2001;42:5293–5296.
19. Bartczak Z, Cohen RE. Argon AS. Evolution of the crystalline texture of high-density polyethylene during uniaxial compression. Macromolecules 1992;25:4692–4694.
20. Strobl GR, Hagedorn W. Raman spectroscopic method for determining the crystallinity of polyethylene. J Polym Sci Polym Phys Ed 1978;16:1181–1193.
21. Rull F, Prieto AC, Casado JM, Sobron F, Edwards HGM. Estimation of crystallinity in polyethylene by Raman spectroscopy. J Raman Spectrosc 1993;24:545–550.
22. Jaynes ET. Information theory and statistical mechanics. Phys Rev 1957;106:620–630.
23. Pérez R, Banda S, Ounaies Z. Determination of the orientation distribution function in aligned single wall nanotube polymer composites by polarized Raman spectroscopy. J Appl Phys 2008;103: 074302.
24. Gurp MV. The use of rotation matrices in the mathematical description of molecular orientations in polymers. Colloid Polym Sci 1995;273:607–625.
25. Barron D, Birkinshaw C. Ultra-high molecular weight polyethylene—Evidence for a three-phase morphology. Polymer 2008;49: 3111–3115.
26. Dumbleton JH, Wang A, Sutton K, Manley MT. Highly crosslinked and annealed UHMWPE. In: Kurtz SM, editor. UHMWPE Biomaterials Handbook, 2nd ed. Amsterdam: Elsevier; 2009. pp 205–219.
27. Wang A, Stark C, Dumbleton JH. Mechanistic and morphological origins of ultra-high molecular weight polyethylene wear debris in total joint replacement prostheses. Proc Inst Mech Engrs H J Eng Med 1996;210:141–155.
28. Wang A, Polineni VK, Essner AP, Sokol M, Sun DC, Stark C, Dumbleton JH. The significance of nonlinear motion in the wear screening of orthopaedic implant materials. J Test Eval 1997;25: 239–245.
29. D'Antonio JA, Manley MT, Capello WN, Bierbaum BE, Ramakrishnan R, Naughton M, Sutton K. Five-year experience with crossfire highly cross-linked polyethylene. Clin Orthop Relat Res 2005;441:143–150.
30. Campbell DG, Field JR, Callary SA. Second-generation highly cross-linked X3^{TM} polyethylene wear: A preliminary radiostereometric analysis study. Clin Orthop Relat Res 2010;468:2704–2709.
31. Thomas GER, Simpson DJ, Mehmood S, Taylor A, McLardy-Smith P, Gill HS, Murray DW, Glyn-Jones S. The seven-year wear of highly croslinked polyethylene in total hip arthroplasty: A double-blind, randomized controlled trial using radiostereoetric analysis. J Bone Joint Surg Am 2011;93:716–722.
32. Nakahara I, Nakamura N, Takao M, Sakai T, Nishii T, Sugano N. Eight-year wear analysis in Longevity highly cross-linked polyethylene liners comparing 26- and 32-mm heads. Arth Orthop Trauma Surg 2011;131:1731–1737.
33. Philip M, Ward IM, Parsons B. A comparison of tensile, compressive and torsional creep in isotropic and oriented polyethylene. J Mater Sci 1986;21:879–886.